Polymer 344 (2026) 129550

Contents lists available at ScienceDirect

Polymer

journal homepage: www.elsevier.com/locate/polymer

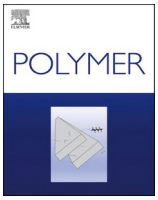

Effect of side chain length on the miscibility and hydrogen bonding interactions of CO_2-based copolymers blending with poly(vinyl phenol) and poly(vinyl chloride)

Min-Jhen Yu, Yen-Ling Kuan, Wei-Ting Du, Shiao-Wei Kuo *

Department of Materials and Optoelectronic Science, Center for Functional Polymers and Supramolecular Materials, National Sun Yat-Sen University, Kaohsiung, 80424, Taiwan

ARTICLE INFO

Keywords:
CO_2-Based copolymers
Hydrogen bonding
Miscibility
And 2D-FTIR

ABSTRACT

In this study, CO_2-based alternating copolymers with different side chain lengths, including poly(propylene carbonate) (PPC), poly(*n*-butyl glycidyl ether carbonate) (P*n*BGEC), poly(*t*-butyl glycidyl ether carbonate) (P*t*BGEC), and poly(2-ethylhexyl glycidyl ether carbonate) (PEHGEC), were successfully synthesized using salen Co-Cl as a catalyst based on FTIR, ^{1}H and ^{13}C NMR spectroscopy, and MALDI-TOF mass spectrometry. The results indicated that increasing the side chain length decreased the glass transition temperature (T_g) and thermal stability, attributed to increased free volume and reduced inter- and intramolecular interactions. The 1D- and 2D-FTIR correlation spectroscopy further demonstrated that intramolecular hydrogen bonding interactions decreased with increasing side chain length, as evidenced by the shifting of C=O absorption peaks and reductions in full width at half maximum (FWHM) values. Additionally, the binary polymer blends of poly(vinyl phenol) (PVPh) with these CO_2-based copolymers were examined to determine their miscibility and intermolecular interactions, indicating that PVPh/PPC and PVPh/P*n*BGEC blends exhibited partially miscible behavior. In contrast, PVPh/P*t*BGEC blends were immiscible. Most interestingly, PVPh/PEHGEC blends exhibited a single T_g, suggesting complete miscibility due to stronger intermolecular hydrogen bonding and free volume effect between PVPh and PEHGEC, as confirmed by FTIR analysis. This result can also be extended to PVC-based binary blends (PVC/P*n*BGEC and PVC/PEHGEC), whose miscibility was weaker compared to blends with PVPh, with the PVC/PEHGEC blend exhibiting a more favorable miscibility behavior due to stronger hydrogen bonding interactions. This study highlights the critical role of side chain length in governing the thermal properties, intermolecular interactions, and miscibility of CO_2-based alternating copolymers, providing valuable insights for designing advanced polymer materials with tailored properties.

1. Introduction

The growing environmental concerns surrounding plastic waste and fossil fuel depletion have driven significant research into the development of bio-based and sustainable polymers [1–3]. There has been a growing interest in developing sustainable polymers from renewable resources, with carbon dioxide (CO_2)-based copolymers emerging as a promising class, which not only utilize CO_2, a greenhouse gas, as a feedstock but also contribute to the reduction of fossil fuel dependency [4–7]. These copolymers are typically synthesized via the ring-opening copolymerization (ROC) of epoxides with CO_2, offering an eco-friendly alternative to traditional petroleum-based plastics [8–13]. This process results in the formation of alternating copolymers with varying properties, including high thermal stability, biodegradability, and tunable mechanical characteristics, making them ideal for applications in packaging, automotive, and biomedical fields [14–19].

To mediate the thermal properties of CO_2-based copolymer, researchers blend them with other polar polymers through intermolecular hydrogen bonding such as starch, cellulose, poly(methyl methacrylate) (PMMA), poly(lactic acid) (PLA), poly(vinyl alcohol) (PVA), poly(vinyl chloride) (PVC), and poly(vinyl phenol) (PVPh) [20–27]. For example, cyclohexene oxide (CHO) was copolymerized with CO_2 to produce poly(cyclohexene carbonate) (PCHC) alternating copolymers or further copolymerized with phthalic anhydride (PA) or 1,

* Corresponding author.
E-mail address: kuosw@faculty.nsysu.edu.tw (S.-W. Kuo).

https://doi.org/10.1016/j.polymer.2025.129550
Received 28 September 2025; Received in revised form 24 December 2025; Accepted 30 December 2025
Available online 31 December 2025

2-cyclohexanedicarboxylic anhydride (CHA) to form CO_2-based poly (carbonate-*co*-ester) (PC-*co*-PE) copolymers. These copolymers were then blended with PVPh to produce miscible binary blends, attributed to strong intermolecular hydrogen bonding interactions. [28]. In addition, Meng et al. have proposed that poly(carbonate-*co*-ester) from propylene oxide (PO) and PA monomers with CO_2 as a plasticizer exhibits complete miscibility with PVC, as evidenced by dynamic mechanical analysis (DMA). [29]. Di-2-ethylhexyl phthalate (DOP), a standard plasticizer with a long alkyl chain, is commonly used in the PVC industry. [30]. As a result, the influence of different side chain lengths on the miscibility and thermal properties of CO_2-based alternating copolymers and blending form with PVC or PVPh was of interest in this study.

To achieve this goal, the choice of epoxide and catalyst plays a significant role in determining the properties of the resulting CO_2-based copolymers. In particular, the structure of epoxide, such as the length of the side chains, can influence physical and chemical properties of the copolymer, including its glass transition temperature (T_g), molecular weight, and intermolecular interactions [31,32]. In this study, we explore the influence of different side chain lengths on the properties of polycarbonate-based alternating copolymers. Specifically, we examine a series of poly(propylene carbonate) (PPC), poly(*n*-butyl glycidyl ether carbonate) (P*n*BGEC), poly(*t*-butyl glycidyl ether carbonate) (P*t*BGEC), and poly(2-ethylhexyl glycidyl ether carbonate) (PEHGEC) copolymers synthesized via the ring-opening copolymerization of CO_2 with their corresponding epoxides using a salen Co-Cl catalyst as shown in Scheme 1.

The influence of side chain length on the thermal stability, molecular interactions, and miscibility of these copolymers is investigated through various techniques, including FTIR, NMR spectroscopy, MALDI-TOF mass spectrometry, differential scanning calorimetry (DSC), thermogravimetric analysis (TGA), and 2D-IR spectroscopy. In addition, the miscibility of binary polymer blends of PVPh or PVC with these CO_2-based copolymers is also evaluated to understand how intermolecular hydrogen bonding affects the phase behavior of these blends. We use a combination of analytical techniques, such as DSC, 1D, and 2D-FTIR spectroscopy, to probe the molecular structure and phase transition of the blends. Of particular interest is the role of intermolecular hydrogen bonding and free volume effect from the different side chain lengths in influencing the miscibility behavior of PVPh or PVC with the CO_2-based copolymers. The aim of this work is to provide a comprehensive understanding of how side chain length impacts the properties of CO_2-based copolymers and their blend. By understanding the factors that govern the miscibility and phase transition of CO_2-based copolymers with PVPh or PVC, we can better tailor the properties of these materials for specific applications, paving the way for the development of new and environmentally friendly polymer blends.

2. Experimental section

2.1. Materials

Propylene oxide (PO, 99.5 %), butyl glycidyl ether (BGE, 99 %), *tert*-butyl glycidyl ether (*t*-BGE, 99 %), and 2-ethylhexyl glycidyl ether (EHGE, 98 %) were stirred with calcium hydride overnight, then distilled under reduced pressure. After purification, the distilled compounds were transferred into Schlenk flasks and stored in a glovebox under an inert atmosphere. (S, S)-(+)-N, N′-Bis(3,5-di-tert-butylsalicylidene)-1,2 cyclohexane diamine cobalt (II) (Salen Co) was dissolved in DCM and subsequently purified by recrystallization from methanol before use. Dichloromethane (DCM, 99 %), tetrahydrofuran (THF, 99.9

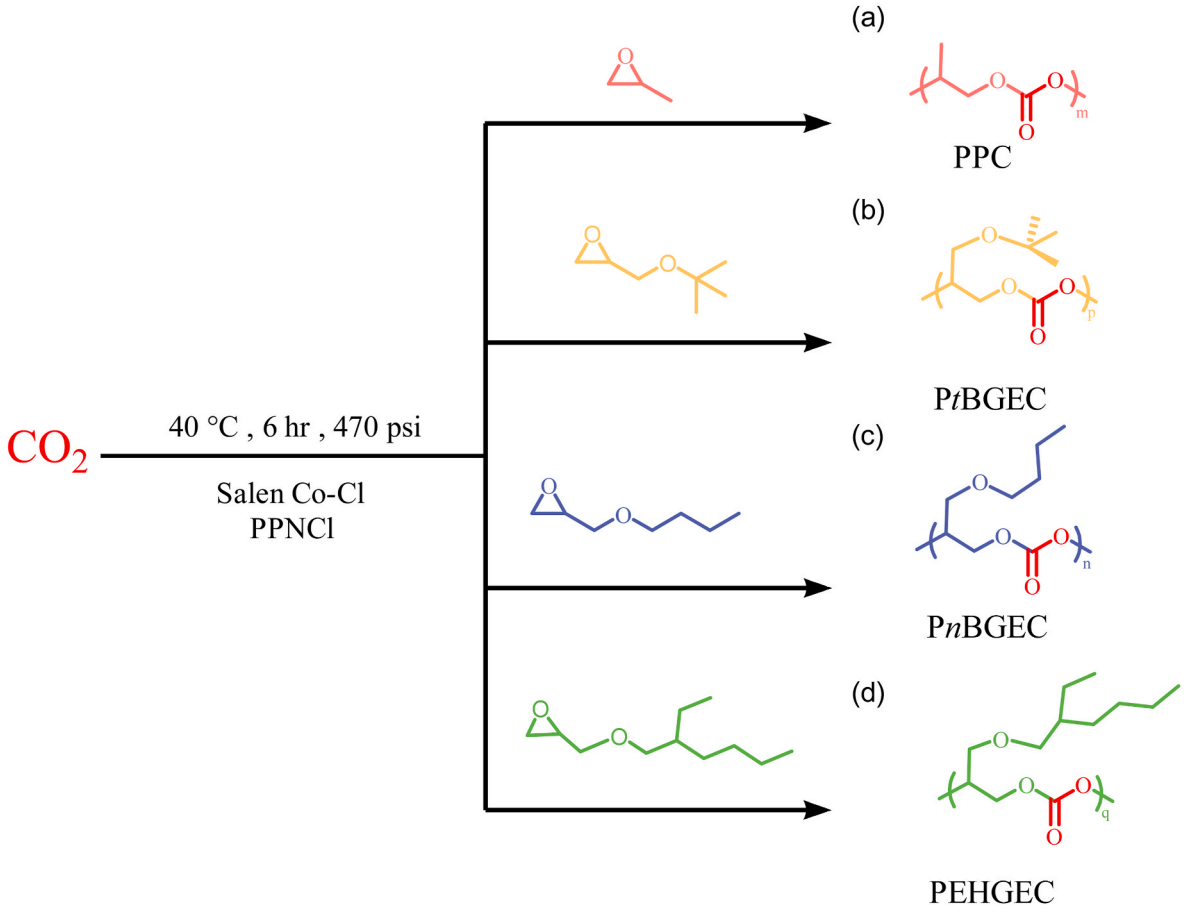

Scheme 1. The synthesis of alternating copolymers of PPC, P*t*BGEC, P*n*BGEC, and PEHGEC.

%), and methanol (MeOH, 99.9 %) were purchased from Acros. Poly (vinyl phenol) (PVPh, Sigma-Aldrich), magnesium sulfate anhydrous ($MgSO_4$, SHOWA), bis(triphenylphosphoranylidene)ammonium chloride (PPNCl, TCI), *p*-toluenesulfonic acid (SHOWA), hydrochloric acid (Alfa-Aesar). Poly(vinyl chloride) (PVC) was purchased from Sigma–Aldrich and used without further purification. The average molecular weight of the PVC used in this study was approximately 90,000, with a polydispersity index (*Đ*) of 2.25, as provided by Sigma–Aldrich. High-purity CO_2 (>99.999 %) was purchased from Hsin E-Li Co., Ltd.

2.2. Synthesis of the salen Co-Cl catalyst [33–36]

Salen-Co (0.4 g) was dissolved in DCM under stirring until a saturated solution was obtained. *p*-TsOH (0.1336 g) was added, and the reaction mixture was stirred magnetically at room temperature for 4 h. Then, most of the DCM was evaporated under reduced pressure, and the crude residue was precipitated by adding pre-cooled hexane. The precipitate was collected by filtration and dried under vacuum, yielding a green powder identified as Salen Co-OTs. ^{1}H NMR (500 MHz, DMSO-d_6, δ, ppm): 1.30 (s, 18H), 1.55–1.61 (m, 2H), 1.74 (s, 18H), 1.87–1.93 (m, 2H), 1.98–2.01 (m, 2H), 2.27 (s, 3H), 3.04–3.08 (m, 2H), 3.58–3.62 (m,2H), 7.09 (d, J = 8.0 Hz, 2H), 7.43–7.47 (m, 6H), 7.81 (s, 2H). Salen Co-OTs (0.3g) was dissolved in DCM under stirring until a saturated solution was obtained and washed with saturated NaCl solution, ensuring complete phase separation. The DCM solution was collected and dried over $MgSO_4$. The drying agent was removed by gravity filtration, and the solvent was evaporated under reduced pressure. The resulting concentrated solution was added dropwise into pre-cooled hexane with stirring, inducing precipitation. The solid was collected by filtration and dried under vacuum, yielding the final product, Salen Co-Cl, as a green powder (yield: 30 %). ^{1}H NMR (500 MHz, DMSO-d_6, δ, ppm):1.31 (s, 18H), 1.54–1.66 (m, 2H), 1.74 (s, 18H), 1.85–1.99 (m, 2H), 1.99–2.10 (m, 2H), 3.03–3.12 (m, 2H), 3.58–3.68 (m, 2H), 7.46 (s, 2H), 7.50 (s, 2H), 7.82 (s, 2H). All characteristics of Salen Co-Cl catalyses were summarized by FTIR and ^{1}H NMR analyses as shown in Fig. S1 and S2.

2.3. Copolymerization of CO_2 and glycidyl ether via ROCOP

The copolymerization of CO_2 and BGE (16 mL) was conducted via ring-opening copolymerization (ROCOP). In a glovebox, BGE, PPNCl (co-catalyst, 64.3 mg), and Salen Co-Cl (catalyst, 71.6 mg) were loaded into a pre-dried reactor, purged with CO_2, and reacted at 40 °C and 470 psi for 6 h. After cooling in an ice bath, the mixture was dissolved in DCM, and CH_3OH was added to terminate the reaction. The catalyst was removed via extraction with 5 wt% HCl solution, and the organic layer was dried over $MgSO_4$. The purified solution was precipitated into pre-chilled methanol, filtered, and dried under high vacuum at 40 °C for 24 h, yielding a honey-like polymer poly(*n*-butyl glycidyl ether carbonate) (P*n*BGEC). P*n*BGEC: ^{1}H NMR (500 MHz, $CDCl_3$, δ, ppm): 5.01 (-C**H**CH_2OCO_2-), 4.22–4.47 (-CHC**H$_2$**OCO_2-), 3.62 (-C**H$_2$**$OCH_2CH_2CH_2CH_3$), 3.44 (-CH_2OC**H$_2$**$CH_2CH_2CH_3$), 1.55 (-CH_2OCH_2C**H$_2$**CH_2CH_3), 1.35 (-$CH_2OCH_2CH_2$C**H$_2$**CH_3), 0.89 (-$CH_2OCH_2CH_2CH_2$C**H$_3$**). ^{13}C NMR (125 MHz, $CDCl_3$, δ, ppm): 154.1 (**C**=O), 74.3 (-CH**C**H_2OCO_2-), 71.4 (-**C**HCH_2OCO_2-), 68.1 (-CH_2O**C**$H_2CH_2CH_2CH_3$), 66.0 (-**C**$H_2OCH_2CH_2CH_2CH_3$), 31.4 (-CH_2OCH_2**C**$H_2CH_2CH_3$), 19.0 (-$CH_2OCH_2CH_2$**C**H_2CH_3), 13.7 (-$CH_2OCH_2CH_2CH_2$**C**H_3). FTIR (KBr, cm^{-1}): 1750 (C=O). Yield: 54.31 %. Following the same procedure and molar ratios, poly(propylene carbonate) (PPC), poly(*t*-butyl glycidyl ether carbonate) (P*t*BGEC), and poly(2-ethylhexyl glycidyl ether carbonate) (PEHGEC) were synthesized.

PPC: ^{1}H NMR (500 MHz, $CDCl_3$, δ, ppm): 4.99 (-C**H**$(CH_3)CH_2OCO_2$-), 4.11–4.29 (-CH(CH_3)C**H$_2$**OCO_2-), 1.34 (-CH(C**H$_3$**$)CH_2OCO_2$-). ^{13}C NMR (125 MHz, $CDCl_3$, δ, ppm): 154.1 (**C**=O), 72.3 (-CH(CH_3)**C**H_2OCO_2-), 68.9 (-**C**H$(CH_3)CH_2OCO_2$-), 16.1 (-CH(**C**$H_3)CH_2OCO_2$-). FTIR (KBr, cm^{-1}): 1750 (C=O). Yield: 49.16 %. P*t*BGEC: ^{1}H NMR (500 MHz, $CDCl_3$, δ, ppm): 4.94 (-C**H**CH_2OCO_2-), 4.22–4.47 (-CHC**H$_2$**OCO_2-), 3.53 (-CH_2OC**H**$(CH_3)_3$), 1.17 (-CH_2OCH(C**H$_3$**$)_3$). ^{13}C NMR (125 MHz, $CDCl_3$, δ, ppm): 154.3 (**C**=O), 74.9 (-CH**C**H_2OCO_2-), 73.5 (-**C**HCH_2OCO_2-), 66.3 (-**C**H_2OCH$(CH_3)_3$), 59.6 (-CH_2O**C**H$(CH_3)_3$), 27.2 (-CH_2OCH(**C**$H_3)_3$). FTIR (KBr, cm^{-1}): 1750 (C=O). Yield: 31.27 %. PEHGEC:^{1}H NMR (500 MHz, $CDCl_3$, δ, ppm): 5.00 (-C**H**CH_2OCO_2-), 4.17–4.47 (-CHC**H$_2$**OCO_2-), 3.58 (-CH_2OC**H$_2$**CH(-$(CH_2)_3CH_3$)CH_2CH_3), 3.33 (-C**H$_2$**OCH_2CH(-$(CH_2)_3CH_3$)CH_2CH_3), 1.57 (-CH_2OCH_2C**H**(-$(CH_2)_3CH_3$)CH_2CH_3), 1.41 (-CH_2OC**H$_2$**CH(-$(CH_2)_3CH_3$)C**H$_2$**CH_3), 1.48, 1.31, 1.26 (-CH_2OCH_2CH(-(C**H$_2$**$)_3CH_3$)CH_2CH_3), 0.89 (CH_3 -CH_2OCH_2CH(-$(CH_2)_3CH_3$)CH_2C**H$_3$**), 0.83 (CH_3 -CH_2OCH_2CH(-$(CH_2)_3$C**H$_3$**)CH_2CH_3). ^{13}C NMR (125 MHz, $CDCl_3$, δ, ppm): 154.2 (**C**=O), 74.8 (-CH**C**H_2OCO_2-), 74.6 (-**C**HCH_2OCO_2-), 68.5 (-CH_2O**C**H_2CH(-$(CH_2)_3CH_3$)CH_2CH_3), 66.1 (-**C**H_2OCH_2CH(-$(CH_2)_3CH_3$)CH_2CH_3), 39.5 (-CH_2OCH_2**C**H(-$(CH_2)_3CH_3$)CH_2CH_3), 30.4, 29.0, 23.7 (-CH_2OCH_2CH(-(**C**$H_2)_3CH_3$)CH_2CH_3), 23.0 (-CH_2OCH_2CH(-$(CH_2)_3CH_3$)**C**H_2CH_3), 14.0 (-CH_2OCH_2CH(-$(CH_2)_3CH_3$)CH_2C**H$_3$**), and 11.0 (-CH_2OCH_2CH(-$(CH_2)_3$C**H$_3$**)CH_2CH_3). FTIR (KBr, cm^{-1}): 1750 (C=O). Yield: 58.79 %.

2.4. Preparation for binary polymer blends

Binary polymer blends were prepared by adding PVPh or PVC along with different CO_2-based copolymers into a flask, followed by dissolution in THF to obtain a 5 wt% solution. The solution was left to evaporate at room temperature for three days, then placed in a vacuum oven at 40 °C for an additional three days to ensure complete solvent removal.

3. Results and discussion

3.1. The synthesis of CO_2-based alternating copolymers

To explore the influence of polycarbonate with different side chains to intermolecular hydrogen bonding interactions, alternating copolymers of poly(propylene carbonate) (PPC), poly(*n*-butyl glycidyl ether carbonate) (P*n*BGEC), poly(*t*-butyl glycidyl ether carbonate) (P*t*BGEC), and poly(2-ethylhexyl glycidyl ether carbonate) (PEHGEC) were synthesized by using salen Co-Cl as a catalyst, as shown Scheme 1. To analyze the influence of the length of the side chains on the interaction between polymers, the copolymers with different lengths of side chains were chosen compared to pure PPC. The copolymerization reaction was carried out at 470 psi of CO_2 at 40 °C for 6 h; all results were summarized in Table 1. It can be observed that the conversion decreases markedly with increasing side-chain length. This indicates that the side-chain length has a noticeable influence on the conversion rate, as shown in Figures S3-S6. Copolymers were found to have remarkable selectivity and the absence of polyether segments. Epoxy conversion was reduced as the side chain length increased, and the side chains led to a decline in epoxy. It was found that the molecular weight decreased from 21,200 to 15,700 from PPC to PEHGEC. This phenomenon is associated with the previously discussed decrease in conversion caused by side chains, which in turn influences the molecular weight of the copolymer. The GPC results of the copolymers, PVPh and PVC are presented in Figs. S7–S12 and Table 1.

The chemical structures of these copolymers were characterized by FTIR, ^{1}H NMR, and ^{13}C NMR spectroscopy, as shown in Fig. 1. The C=O units appear at 1752 cm^{-1} in the FTIR spectrum (Fig. 1(b)), which represents the carbonate groups produced by CO_2 and epoxy units. The other aliphatic CH stretching vibration was at 2970-2830 cm^{-1}, and the C-O was found at ca. 1230 cm^{-1}. In addition, the typical peaks of protons (peak *a*) within the polycarbonate appeared at ca. 5.0 ppm in ^{1}H NMR spectra due to the C**H**$(CH_3)CH_2OCO_2$ of the PPC on the main chain as displayed in Fig. 1(c). In addition, the characteristic peaks of the C=O group also appeared at ca. 154.0 ppm in the ^{13}C NMR as shown in Fig. 1 (d). Similarly, P*n*BGEC, P*t*BGEC, and PEHGEC exhibit similar signals to PPC, and the assignments of the other peaks, based on Fig. 1(a), are summarized in Fig. 1(c) and (d). Furthermore, the successful synthesis of

Table 1
Ring Opening Polymerization of various epoxides with CO_2 Catalyzed by Salen Co-Cl.

Polymer[a]	Conv.(%)[b]	%PC[c]	TON[d]	TOF (h^{-1})[e]	%Select.[f]	T_g[g]	T_{d10}[h]	M_n[i]	$Đ$[i]	FWHM[j]
PPC	90.5	>99	1810	302	15.07	35	305	21,200	1.34	46
PtBGEC	88.6	>99	1770	295	>99	34	252	19,400	1.05	43
P*n*BGEC	63.7	>99	1274	212	>99	−26	283	17,400	1.11	30
PEHGEC	68.5	>99	1370	228	>99	−38	296	15,700	1.18	26

[a] Polymerization conditions: [mono]:[cat]:[co-cat] = 1000:1:1.
[b] Determined by ^{1}H NMR analysis of the crude product.
[c] PC = polycarbonate. The compositions were estimated according to the ^{1}H NMR spectra.
[d] Turnover number (TON) = polymer (g)/catalyst (g).
[e] Turnover frequency (TOF) = TON/time (hours).
[f] Selectivity towards polymer over cyclocarbonate calculated from ^{1}H NMR spectrum.
[g] Determined by DSC analyses.
[h] Determined by TGA analyses.
[i] Determined by GPC in THF, calibrated with narrow molar mass polystyrene standards.
[j] Full width at half maximum (FWHM) of the C=O peak in FTIR.

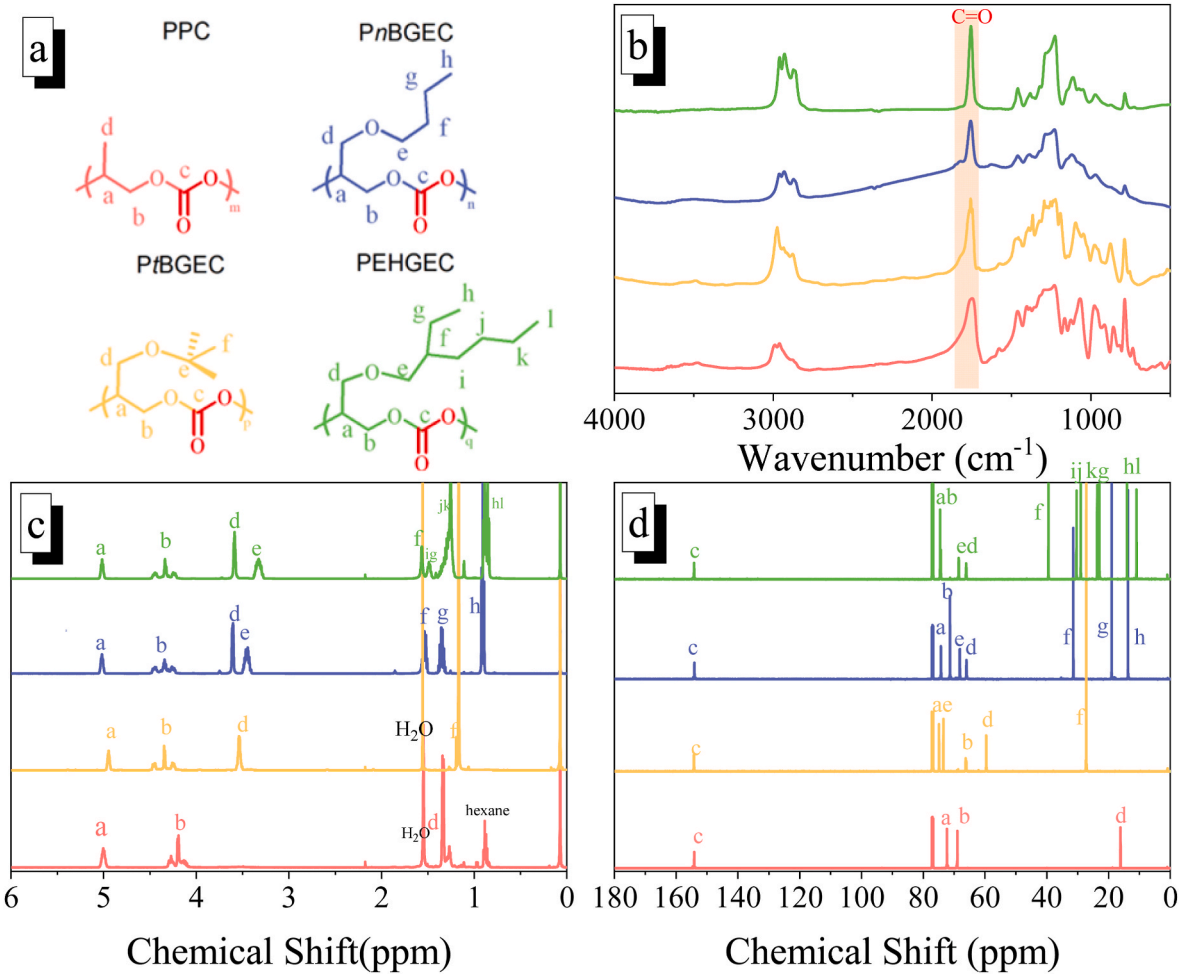

Fig. 1. (a) The chemical structure and the peak assignment of these CO_2-based copolymers, and their corresponding (b) FTIR, (c) ^{1}H NMR, and (d) ^{13}C NMR spectra.

CO_2-based copolymers with different side-chain lengths was confirmed by comparing the COSY NMR and ^{13}C DEPT spectra (Figs. S13–S20).

To investigate the copolymer compositions, we recorded MALDI-TOF mass spectra as shown in Fig. 2. The difference between the signals at 3480.187 and 3378.575 m/z was approximately 102 g/mol, equivalent to one CO_2 molecule plus one propylene oxide molecule. Likewise, it could be found that the repeating units were composed of butyl glycidyl ether/CO_2, *tert*-butyl glycidyl ether/CO_2, and 2-ethylhexyl glycidyl ether/CO_2 at ca. 174, 174, and 230 g/mol, respectively. Hence, it can be confirmed from the above MALDI-TOF mass analyses that PPC, P*t*BGEC, P*n*BGEC, and PEHGEC are all alternating copolymers. In addition, the signals other than the main peak can be attributed to polymer fragments. In Fig. 2(a), besides the repeating unit signal of PPC, the difference of 15 g/mol between the peaks at 3480.187 and 3495.086 m/z (orange line) corresponds precisely to the mass of a $–CH_3$ side chain. Moreover, the mass difference between 3480.187 and 3525.17 m/z (purple line) matches exactly one CO_2 unit. As can be observed in Fig. 2(b), the mass difference between the peak at 2624.170 m/z (orange line) and the main

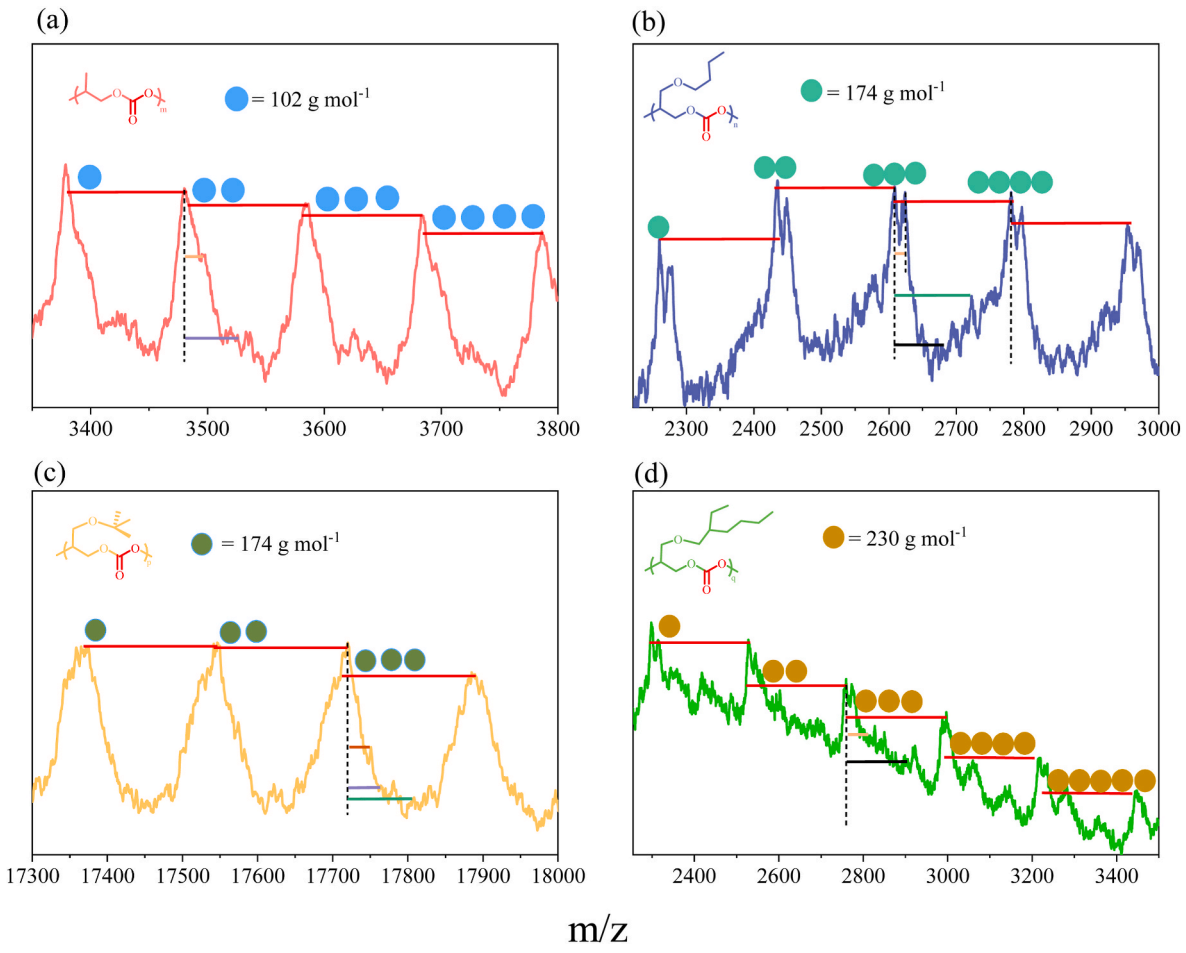

Fig. 2. MALDI-TOF mass spectra of (a) PPC, (b) P*n*BGEC, (c) P*t*BGEC, and (d) PEHGEC.

peak at 2608.376 m/z is 15.794 g/mol, which corresponds precisely to the -CH_3 terminus of the side chain. The mass difference between the peak at 2722.696 m/z (green line) and the main peak is 114.317 g/mol, attributable to the absence of a carbonate group. Similarly, the mass difference between the peak at 2679.539 m/z (black line) and the main peak is 71.162 g/mol, consistent with the presence of a butyl side chain

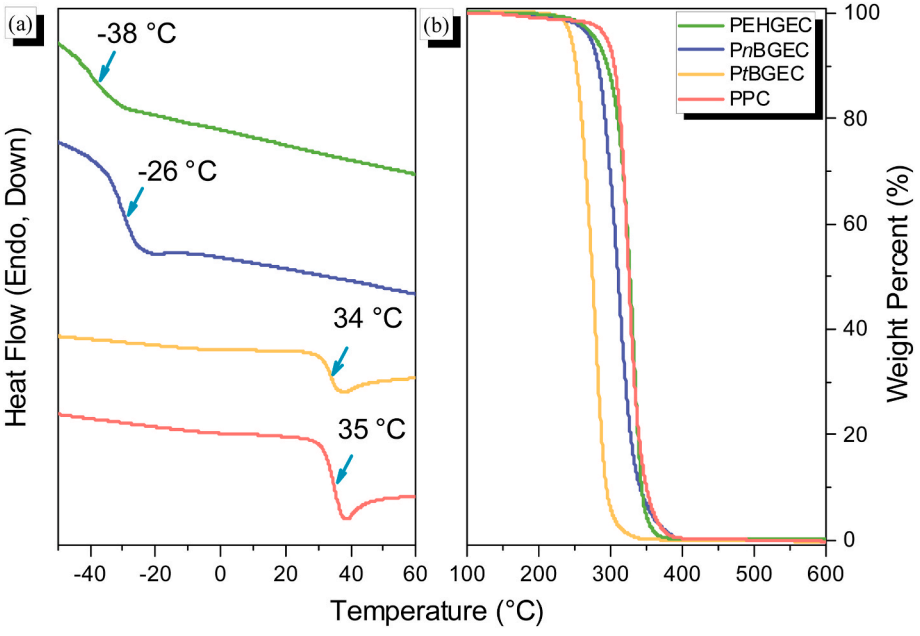

Fig. 3. (a) DSC thermograms and (b) TGA curves of the CO_2-based alternating copolymers.

(-$OCH_2CH_2CH_2CH_3$). In Fig. 2(c), the mass difference between the peaks at 17720.22 and 17750.649 m/z (dark orange line) is approximately 30.4 g/mol, corresponding to the loss of two terminal $–CH_3$ groups in the side chain. Meanwhile, the peak at 17764.649 m/z (purple line) corresponds exactly to the addition of one CO_2 unit. The peak at *m/z* 17808.289 (green line) differs from the main peak by one side chain unit ($–CH_2OC(CH_3)_3$). A similar pattern can be observed in the PHEGEC values shown in Fig. 2(d). The mass difference between 2759.41 and 2803.206 m/z (orange line) corresponds to one unit of carbon dioxide, whereas the difference between 2759.41 and 2901.41 m/z corresponds

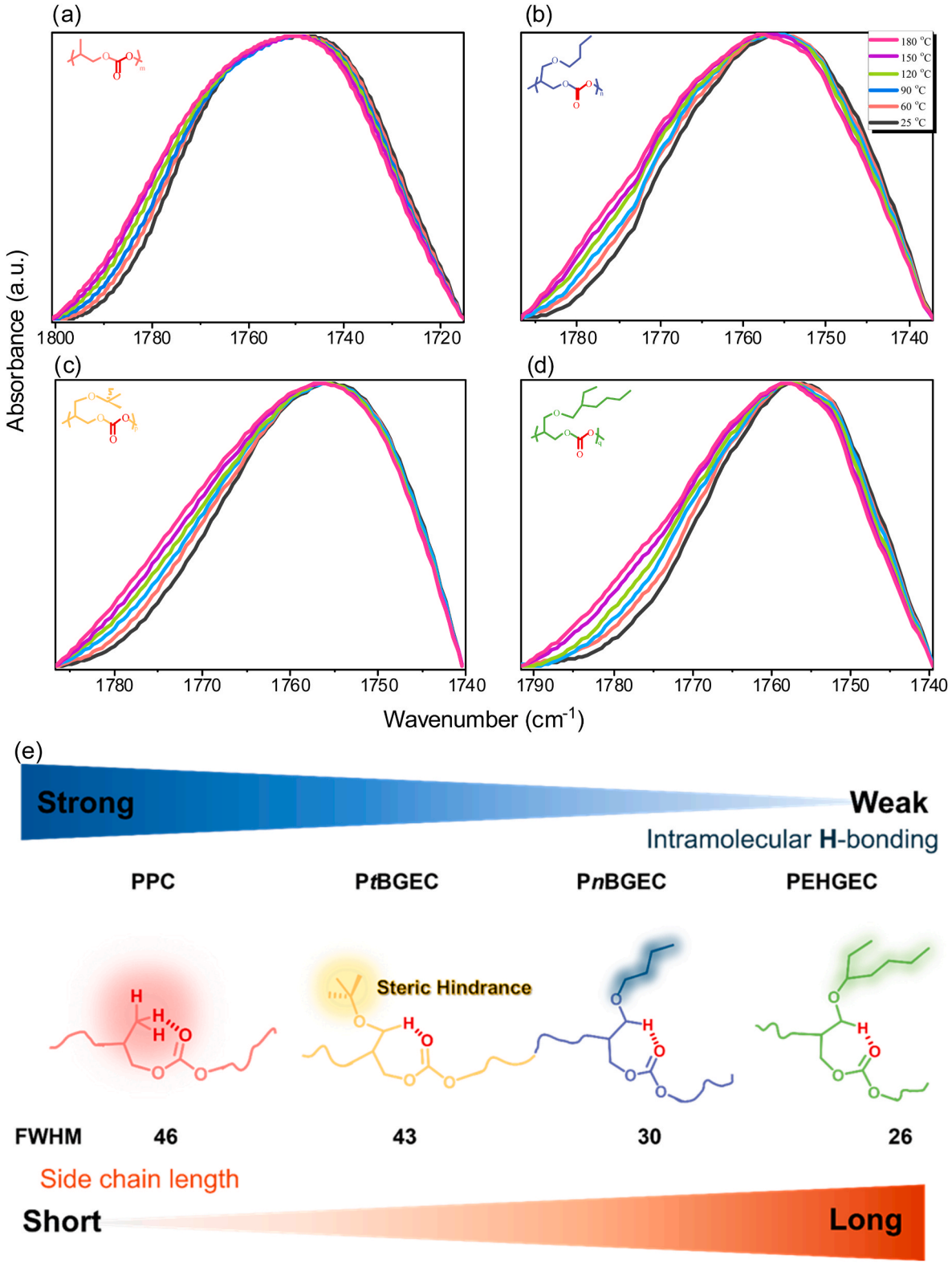

Fig. 4. Temperature-dependent FTIR spectra of (a) PPC, (b) P*n*BGEC, (c) P*t*BGEC, and (d) PEHGEC and (e) the effect of side chain length on the intramolecular hydrogen bonding of these CO_2-based copolymers.

to side chain.

These CO_2-based alternating copolymers were also analyzed by using DSC and TGA analyses, as displayed in Fig. 3. Fig. 3(a) displays the DSC thermograms of these four CO_2-based alternating copolymers, and all copolymers exhibited a single glass transition temperature (T_g). In general, the T_g values of the copolymers decreased as the length of the side chains increased. The molecular chains are spaced wider apart because longer side chains offer more free volume, reduce the intermolecular interaction, and allow the molecules to move more easily. The T_g value of P*t*BGEC was almost the same as the PPC (ca. 35 °C), because the side chain of P*t*BGEC was *t*-butyl group, the *tert*-butyl produces a steric effect that makes the polymer chain tough. When the side chain becomes a linear chain, the T_g value is down to −26 °C °C. As the length of the side chain reaches eight carbons, the T_g value even drops to −36 °C. Furthermore, it was discovered that the P*t*BGEC, P*n*BGEC, and PEHGEC have lower thermal stability than PPC when the copolymers have a longer side chain, which makes them softer. Apart from this, the *t*-butyl group of the P*t*BGEC has large steric hindrance, and the thermal stability of P*t*BGEC was weaker than that of other copolymers, as shown in Fig. 3(b). All thermal properties of these CO_2-based alternating copolymers are also summarized in Table 1.

In our previous studies [37], we have understood that the full width at half maximum (FWHM) of the C=O unit of CO_2-based copolymers and other polymers with C=O units was strongly dependent on the dipole-dipole and hydrogen bonding interactions. Fig. 4 displays all corresponding temperature-dependent FTIR spectra of these CO_2-based copolymers. Clearly, these C=O absorptions all exhibited asymmetric curves, and at least two peaks could be expected from the second-derivative spectra, corresponding to free C=O at relatively higher wavenumber (ca. 1775-1778 cm^{-1}) and intramolecular hydrogen-bonded [C–H···O=C] units at relatively lower wavenumber (ca. 1752-1756 cm^{-1}).

Firstly, the intramolecular hydrogen bonded C=O of PPC was located at ca. 1752 cm^{-1} and this peak was slightly shifted to higher wavenumber as the side chain increased such as 1752 cm^{-1} for P*t*BGEC, 1754 cm^{-1} for P*n*BGEC, and 1756 cm^{-1} for PEHGEC, indicating that the intramolecular hydrogen bonded C=O was slightly destroyed as the side chain length increased. In addition, the FWHM listed in Table 1 was decreased from 46, 43, 30, and 26 cm^{-1} as the length of the side chain increased for PPC, P*t*BGEC, P*n*BGEC, and PEHGEC, respectively, and the scheme was shown in Fig. 4(e). The presence of side chains strongly affects the intramolecular interaction between these CO_2-based copolymer chains. We also observed that the peak positions of intramolecular hydrogen-bonded C=O units were shifted to higher wavenumber, and the fraction of free C=O was increased upon increasing the temperature for all CO_2-based copolymers as displayed in Fig. 4, implying that these interactions were sensitive to temperature perturbations. We also understood that the experimental data of this weak [C–H···O=C] hydrogen bonding is difficult to determine since this interaction usually coexists with other strong hydrogen-bonded C=O units [37]. As a result, 2D-FTIR correlation spectroscopy [38–41] was used to understand this intramolecular hydrogen bonding interaction based on one-dimensional IR spectra (Fig. 4), which responds to spectral perturbations from the temperature change as shown in Fig. 5.

In general, the 2D synchronous spectra were symmetrical with respect to the diagonal line on the correlation map, and the positive (red) and negative (blue) cross-peaks were used in this study. Clearly, all negative cross-peaks were observed in Fig. 5, indicating that these two peaks vary in opposite directions under temperature perturbation. This result implied that these two absorption peaks could be assigned free C=O groups at relatively higher wavenumber (1775-1778 cm^{-1}), and the other is intramolecular hydrogen-bonded C=O at relatively lower

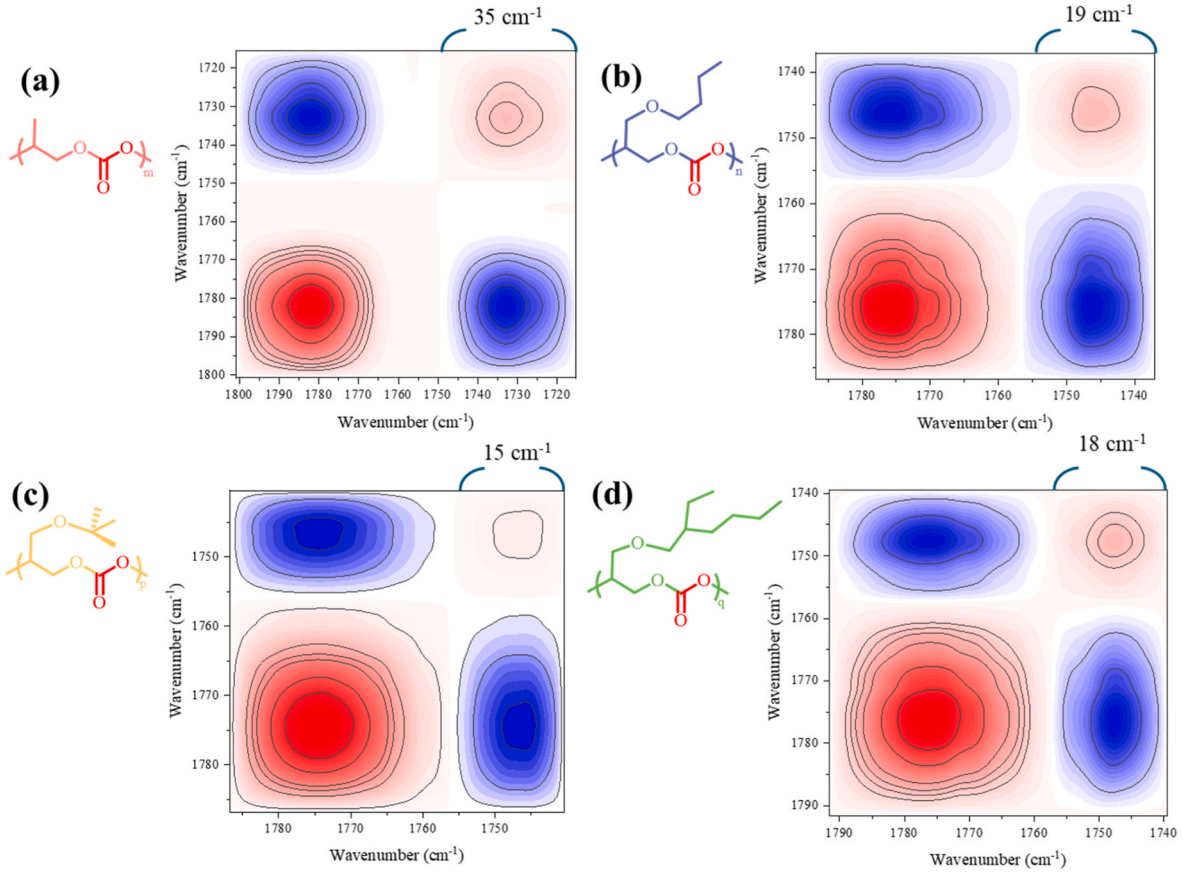

Fig. 5. 2D FTIR synchronous correlation maps of (a) PPC, (b) P*n*BGEC, (c) P*t*BGEC, and (d) PEHGEC.

wavenumber (1752-1756 cm^{-1}), which are varied in opposite directions as expected. Furthermore, the full width of intramolecular hydrogen-bonded C=O units was also strongly dependent on the side chain length, and it was decreased from 35, 19, 15, and 18 cm^{-1} as the length of the side chain increased for PPC, P*n*BGEC, P*t*BGEC, and PEHGEC, respectively. In summary, the synthesis of all these CO_2-based alternating copolymers was successful in this study based on FTIR, NMR, and MALDI-TOF mass spectra analyses. In addition, the thermal stability and intramolecular hydrogen bonding were strongly dependent on the side chain length, which typically decreased upon increasing the length of the side chain based on DSC, TGA, and FTIR analyses.

3.2. *Binary polymer blends of PVPh with CO_2-based alternating copolymers*

DSC thermal analyses are widely used to evaluate the miscibility of polymer blends by analyzing their glass transition behavior. Fig. 6 shows DSC thermograms of PVPh with these four CO_2-based alternating copolymers binary blends. The pure PVPh homopolymer exhibited the T_g value of 168 °C, and pure PPC, P*n*BGEC, P*t*BGEC, and PEHGEC copolymers exhibited single T_g values of 35 °C, 34 °C, −26 °C, and −38 °C, respectively, as mentioned previously. In PVPh/PPC binary blends as shown in Fig. 6(a), the PVPh/PPC = 90/10 blend displays a single T_g value of 151 °C, which is close to the value predicted by the Fox equation (150 °C), indicating this blend composition is miscible. Further increasing PPC compositions, the T_g was maintained at 152 °C and 149 °C for PVPh/PPC = 80/20 and 70/30 blend compositions. The T_g behavior of the PPC domain was not observed due to lower concentrations in these two compositions. However, increasing PPC compositions at 40 wt% and 50 wt% in PVPh/PPC binary blends, both blends clearly exhibited two T_g values, where PVPh major phases still exhibited T_g values at 148 °Cand 150 °C, and PPC major phases were increased from 35 °C to 42 °C and 82 °C, respectively.

All results indicate that the PVPh/PPC blend is a partially miscible system, and all T_g values are summarized in Fig. 7(a). In PVPh/P*n*BGEC binary blends as shown in Fig. 6(b), the PVPh/P*n*BGEC = 90/10 blend also displays a single T_g value of 140 °C, which is also close to the value predicted by the Fox equation (136 °C) [42], indicating this blend composition is miscible. However, increasing P*n*BGEC compositions in PVPh/P*n*BGEC binary blends, both blends clearly exhibited two T_g values, where PVPh major phases increased the Tg value to 146–149 °C, and P*n*BGEC major phases were located between −18 and −26 °C. These results indicated that PVPh/P*n*BGEC binary blends tend to exhibit immiscible behavior at relatively higher PnBGEC compositions

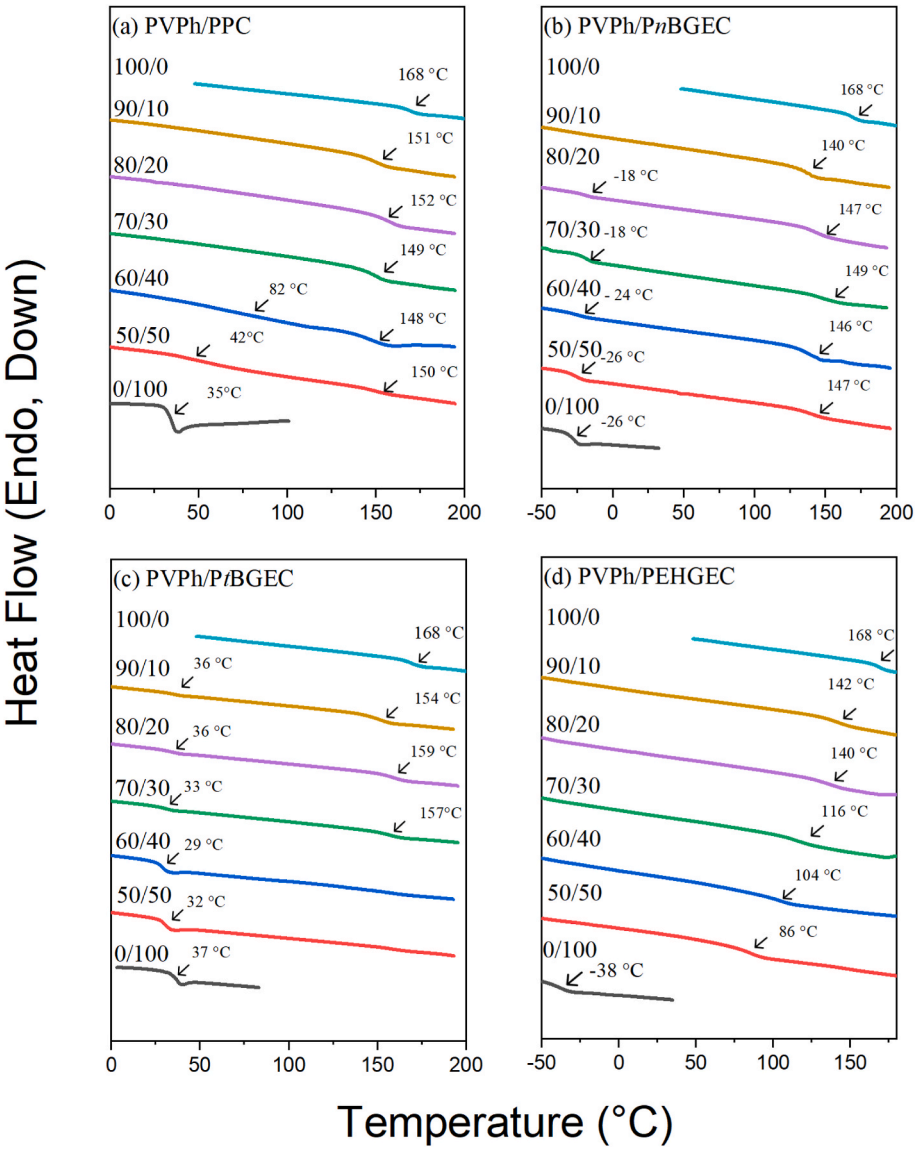

Fig. 6. DSC thermal analyses of (a) PVPh/PPC, (b) PVPh/P*n*BGEC, (c) PVPh/P*t*BGEC, and (d) PVPh/PEHGEC binary blends.

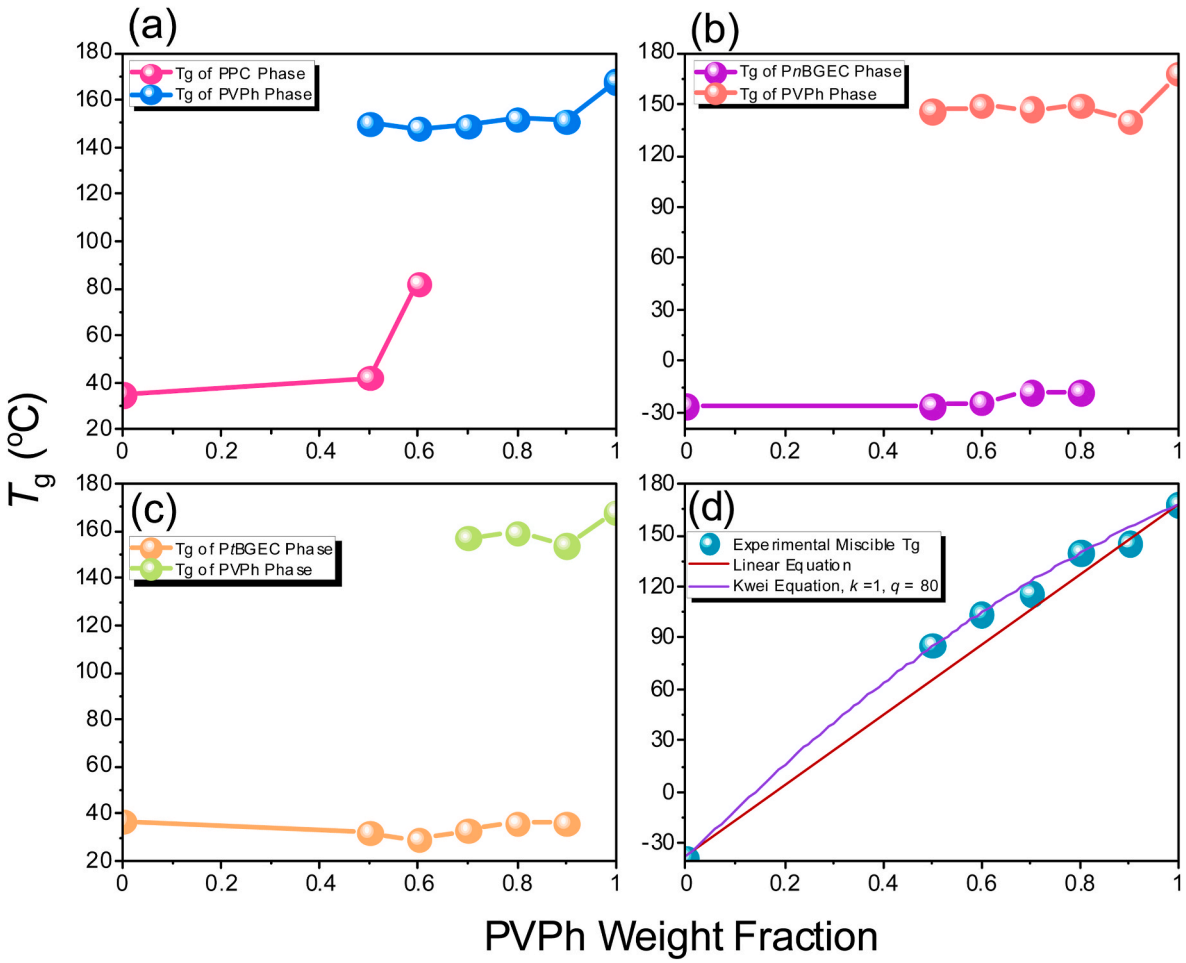

Fig. 7. Summarized T_g values of (a) PVPh/PPC, (b) PVPh/P*n*BGEC, (c) PVPh/P*t*BGEC, and (d) PVPh/PEHGEC binary blends, where the single T_g values are also predicted by the linear and the Kwei equations.

compared with PVPh/PPC blends, and all T_g values are summarized in Fig. 7(b). Fig. 6(c) displays DSC thermal analyses of PVPh/P*t*BGEC binary blends and all blend compositions exhibited two T_g values, where PVPh major phases displayed T_g value at 154–157 °C and P*t*BGEC major phases were located at 29–36 °C, indicating that this binary blend is totally immiscible behavior and all T_g values are also summarized in Fig. 7(c). Most importantly, Fig. 6(d) displays DSC thermal analyses of PVPh/PEHGEC binary blends, and all blend compositions exhibited one single T_g value, suggesting that this binary blend is miscible. The Fox equation generally could predict the T_g value of composition-dependent systems; however, the Kwei equation is typically used for hydrogen-bonded miscible polymer blends [43]. As shown in Fig. 7(d), the q value in the Kwei equation for PVPh/PEHGEC blend is 80 and k = 1, which is much higher than our previous studies in PVPh with other CO_2-based copolymers [28,37]. This result also implies that the PVPh/PEHGEC blend may have stronger intermolecular interactions than other CO_2-based copolymers, which could enhance the thermal properties and miscibility. We calculated the K_A values (K_A = 10) of the PVPh/PEHGEC binary blends using the Painter–Coleman association model, and the corresponding thermodynamic parameters are summarized in Table S1. As shown in Fig. S21, the K_A values are significantly lower than the K_B values, suggesting that the intermolecular hydrogen bonds are weaker than those in pure PVPh. This result is consistent with the negative q value obtained from the Kwei equation.

The intermolecular interactions could be identified by FTIR spectroscopy both qualitatively and quantitatively in the solid state [44–48]. According to the second-derivative spectra shown in Fig. S22, three signals appear at approximately 1770, 1760, and 1745 cm^{-1}, which can be assigned to free C=O, intramolecularly hydrogen-bonded C=O, and intermolecularly hydrogen-bonded C=O, respectively. Fig. 8 shows the FTIR spectral regions about C=O units of PVPh with these four CO_2-based alternating copolymers binary blends at room temperature. In PVPh/PPC binary blends as shown in Fig. 8(a), pure PPC shows the peak at ca. 1752 cm^{-1}, and the FWHM is ca. 46 cm^{-1}. As increasing the PVPh compositions in PVPh/PPC blends, the peak was slightly shifted to higher wavenumber from 1752.0 to 1753.5, 1757.3, 1757.3, 1757.8, and 1758.8 cm^{-1} and the FWHM was decreased from 46.7 to 43.3, 42.9, 40.9, 40.0, and 37.6 cm^{-1} for PVPh/PPC = 0/100, 50/50, 60/40, 70/30, 80/20 and 90/10, respectively, as shown in Fig. 9(a).

Consequently, the intramolecular hydrogen bonding of PPC was destroyed, and the intermolecular hydrogen bonding between the PVPh and PPC segments tends to decrease upon increasing PVPh compositions. As a result, the PVPh/PPC blends show partially miscible behavior as shown in Fig. 7(a). Fig. 8(b) presents FTIR spectra of PVPh/P*n*BGEC binary blends recorded at room temperature, where all blend compositions exhibited the same peak position at ca. 1754 cm^{-1}; however, the FWHM was decreased from 31.8 to 27.9 and 26.3 cm^{-1} for PVPh/P*n*BGEC = 0/100, 50/50, and 60/40 binary blends. Further increasing the PVPh compositions to 70–90 wt%, the FWHM was maintained at 26.3 cm^{-1} as shown in Fig. 9(b). Clearly, both PVPh/PPC and PVPh/P*n*BGEC binary blends are classified into the weak intermolecular hydrogen bonding interaction system, and both blends could be treated as two separate parts with a large T_g difference, such as 133 °C for PVPh/PPC and 194 °C for PVPh/P*n*BGEC binary blends.

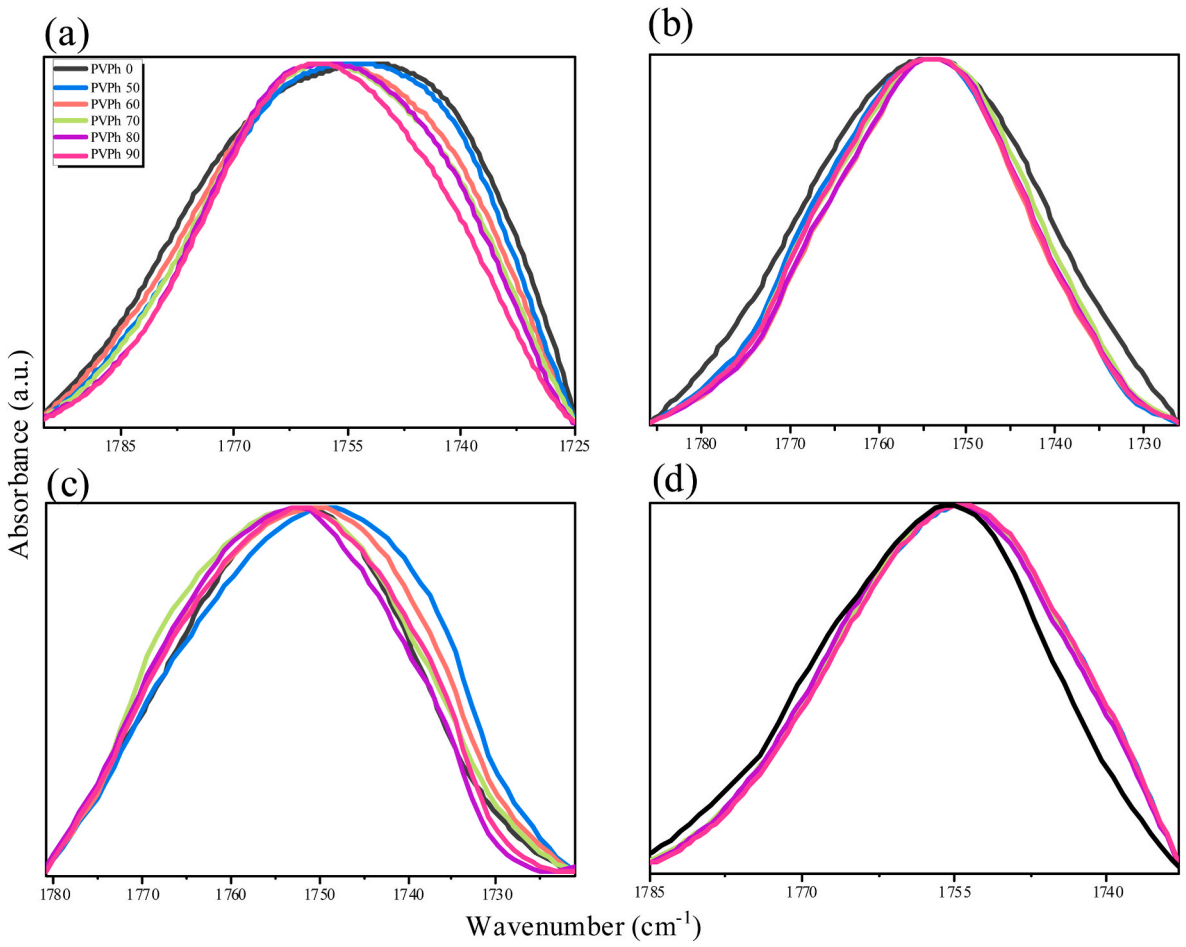

Fig. 8. FTIR spectra recorded at room temperature of (a) PVPh/PPC, (b) PVPh/P*n*BGEC, (c) PVPh/P*t*BGEC, and (d) PVPh/PEHGEC binary blends.

At relatively low PVPh compositions (<80 wt%), because of weakening hydrogen bonding and the decoupling of segment motion by fast dynamics, resulting in a decrease in T_g value. Kratochvil et al. proposed the predominance of weak interaction and strong involvement of conformational entropy at lower PVPh compositions, and if the enthalpic energy effect is only relevant, the phase separation would occur [49]. At relatively higher PVPh compositions (90 wt%), the conformation entropy effects are suppressed because of reduced mobility of hydrogen-bonded segments, which enhances the miscibility in both PVPh/PPC and PVPh/P*n*BGEC binary blends. In addition, Fig. 8 (c) exhibits FTIR spectra of PVPh/P*t*BGEC binary blends measured at room temperature where the peak was firstly shifted to lower number from 1752.0 to 1749.1 cm^{-1} and then shifted to higher wavenumber to 1750.1, 1752.0, 1752.0 and 1753.0 cm^{-1} and the FWHM was also increased from 30.8 to 36.2 cm^{-1} and then decreased to 35.3, 35.2, 34.2, and 33.9 cm^{-1} for PVPh/P*t*BGEC = 0/100, 50/50, 60/40, 70/30, 80/20 and 90/10, respectively, as shown in Fig. 9(c). Clearly, the weak enthalpic energy is only relevant; the phase separation also occurred at lower PVPh (50 wt%), further increasing the PVPh compositions, the intermolecular hydrogen bonding between PVPh/P*t*BGEC decreased, and thus the conformation entropy effect was dominated, which also resulted in phase separation. As a result, the PVPh/P*t*BGEC binary blend is immiscible for all blend compositions. Finally, Fig. 8(d) shows FTIR spectra of PVPh/PEHGEC binary blends measured at room temperature, where the peak was first shifted to a lower wavenumber from 1756.0 to 1754.4 cm^{-1}, and the FWHM was also increased from 26.1 to 28.1 cm^{-1} for all blend compositions, as shown in Fig. 9(d). Since the similar hydrogen bonding strength for all blend compositions could suppress the conformation entropy effects by their reduced mobility, and the large Tg difference of 206 °C was observed, which induced the totally miscible state for PVPh/PEHGEC binary blends. Overall, Scheme 2 summarizes the self-association hydrogen bonding and intermolecular hydrogen bonding interaction between PVPh with various CO_2-based copolymers, where the long alkyl chain will reduce the self-association hydrogen bonding of PVPh and then enhance the intermolecular hydrogen bonding interaction of PVPh with CO_2-based copolymers observed that PVPh is miscible with poly(methyl methacrylate) (PMMA), poly(ethyl methacrylate) (PEMA), and poly(*n*-propyl methacrylate) (PPMA) for all blend compositions; however, PVPh/poly(*n*-butyl methacrylate) (PBMA) blends display phase separation [50]. The experimental fraction of hydrogen-bonded C=O groups in PVPh/PBMA (C4) blend is much lower than the short side chain of poly(*n*-alkyl methacrylate) (C1-C3), which results in phase separation.

Compared with the PVPh/poly(*n*-alkyl methacrylate) binary blend system, Painter et al. have Therefore, the PVPh/PPC binary blends with short side chain (CH_3) group show better miscibility behavior than those with longer side chain (C_4H_9) group of PVPh/P*t*BGEC and PVPh/P*n*BGEC binary blends. However, the free volume effects would become obvious if the binary blend system had weak hydrogen bonding interactions, which is discussed in the previous study [37]. For example, PVC/phthalate ester blend systems, if the alkyl chain is below C4, which is too high in volatility, but the alkyl chain is higher than C13, which exhibits limited miscibility. As a result, the di-2-ethylhexyl phthalate (DOP) with C8 is still regarded as the standard plasticizer in the industry [30]. Therefore, the PVPh/PEHGEC binary blends were miscible due to the balance between intermolecular hydrogen bonding interactions and the combined effects of free volume and conformational entropy. Based on Table 1, we could observe that the FWHM of PEHGEC shows the

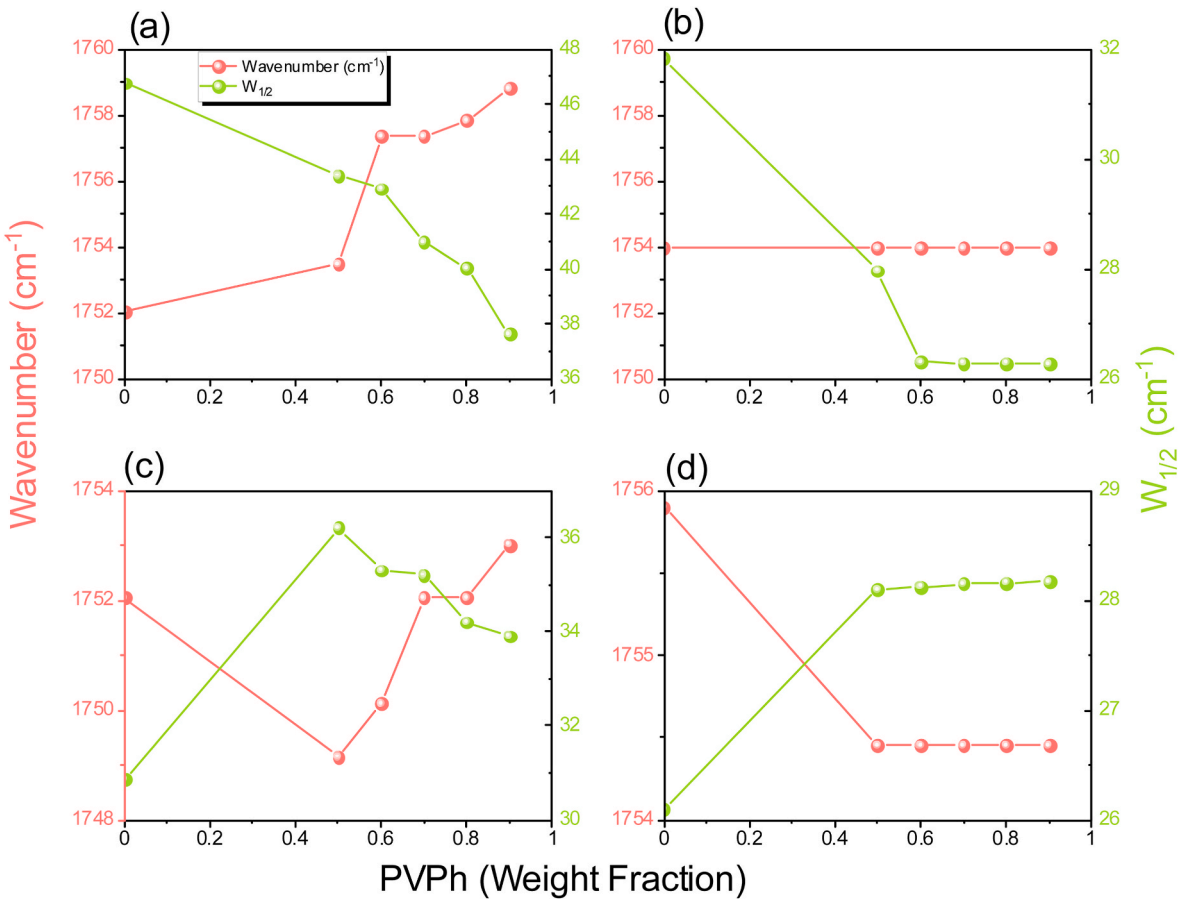

Fig. 9. Peak position and FWHM based on FTIR spectra (Fig. 8) of (a) PVPh/PPC, (b) PVPh/P*n*BGEC, (c) PVPh/P*t*BGEC, and (d) PVPh/PEHGEC binary blends.

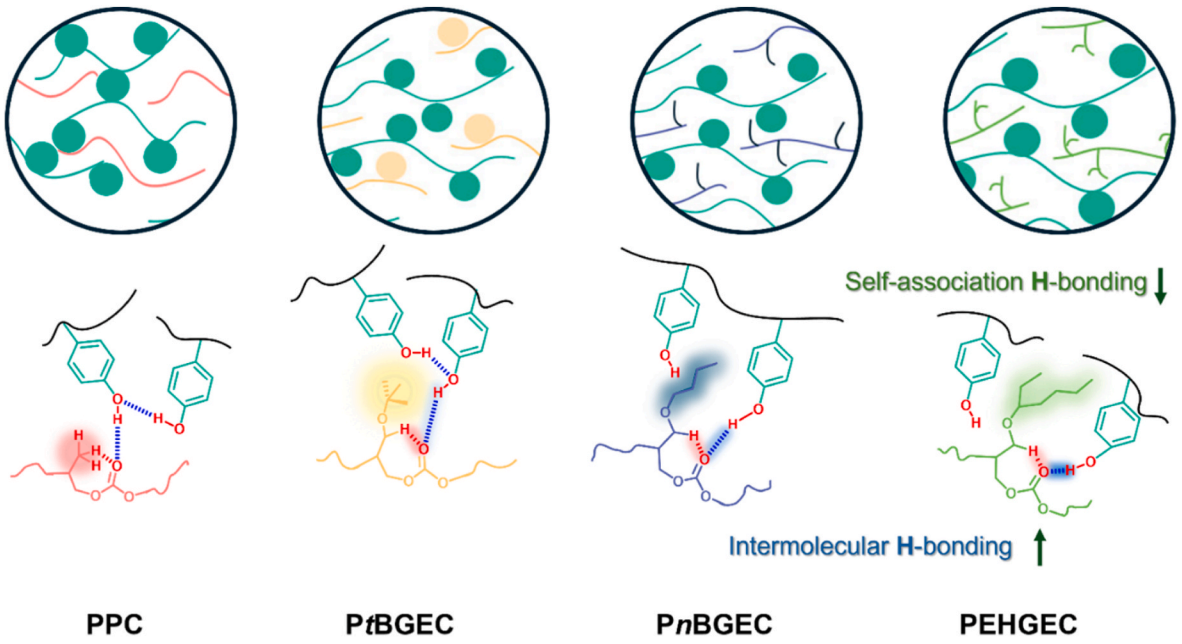

Scheme 2. The scheme about the self-association hydrogen bonding and intermolecular hydrogen bonding interaction between PVPh with various CO_2-based copolymers.

narrowest band of C=O units, indicating that the long side chain (C8) inhibits the self-association of inter-chain or intra-chain hydrogen bonding interactions [C–H···O=C] of pure PEHGEC segment because of the largest free volume. The weakest self-association [C–H···O=C] hydrogen bonding interaction from PEHGEC segments compared with PPC, P*n*BGEC, and P*t*BGEC segments would be as expected. As blending

with PVPh, the weakest self-association [C–H···O=C] hydrogen bonding based on PEHGEC is preferred to interact with the phenolic OH units of PVPh to form the strongest intermolecular [O–H···O=C] hydrogen bonding compared with other CO_2-based copolymers, which is confirmed by FTIR analyses (Figs. 8 and 9). In addition, the long side chain provides the largest free volume effect to suppress the conformation entropy effect and then enhance the miscibility behavior. Based on all DSC and FTIR analyses, we conclude that the PVPh/PEHGEC binary blends possess better miscibility compared with other CO_2-based copolymers.

To further understand the intermolecular hydrogen bonding interaction in PVPh/PEHGEC binary blends, Fig. 10(a) shows FTIR spectra of PVPh/PEHGEC = 50/50 blends recorded at various temperatures, where the C=O signal of PEHGEC was shifted to a higher wavenumber, implying that the intermolecular hydrogen bonding strength decreased with the increase of temperature. 2D FTIR analyses could also provide more effective information in this PVPh/PEHGEC binary blend, as shown in Fig. 10(c) and (d). Similarly, two major bands are also observed in the 2D-FTIR synchronous spectrum (Fig. 10(c)) for C=O units, the band for the free C=O group of PEHGEC is at ca. 1775 cm^{-1}, and the intramolecular or intermolecular hydrogen-bonded C=O unit of PEHGEC or with PVPh is at ca. 1745 cm^{-1}, which is much lower than the 1D-FTIR analyses. Similarly, the negative cross-peaks were observed, implying that these two peaks vary in opposite directions under temperature perturbation, as expected. Fig. 10(d) displays its corresponding 2D-FTIR asynchronous spectrum, and we could conclude that the hydrogen-bonded C=O units were altered before the free C=O units based on Noda's rule because of the correlations being opposite in the synchronous 2D spectrum. The possible hydrogen bonding interaction scheme was summarized in Fig. 10(b).

3.3. Binary polymer blends of PVC with PnBGEC and PEHGEC

We turn our attention to investigating the weaker hydrogen bonding of PVC compared with PVPh, as blending with CO_2-based copolymers. For brevity, we selected PVC/P*n*BGEC and PVC/PEHGEC binary blends with similar T_g behavior of P*n*BGEC (−26 °C) and PEHGEC (−38 °C). Fig. 11(a) and (b) present the DSC thermal analyses of PVC/P*n*BGEC and PVC/PEHGEC binary blends, respectively. The PVC/PnBGEC = 90/10 blend also displays a single Tg value of 42 °C with miscible phase; however, this value is much lower than the predicted by the Fox equation (70 °C) as displayed in Fig. 11(a). This result confirms that the intermolecular hydrogen bonding of PVC/P*n*BGEC is weaker than PVPh/P*n*BGEC, as expected. Further increasing P*n*BGEC compositions, two T_g values were observed where the PVC major phase shifted to a higher T_g value from 55 to 71 °C, and the P*n*BGEC major phase was observed from −28 to −38 °C, indicating these blend compositions are immiscible, which is similar to PVPh/P*n*BGEC blends.

Similarly, Fig. 11(b) shows DSC thermal analyses of PVC/PEHGEC binary blends, where PVC/PEHGEC = 90/10 blend exhibits a single T_g value of 45 °C, which is also much lower than the predicted by Fox equation (67 °C) but is higher than the PVC/P*n*BGEC = 90/10 blend at the same composition even pure PEHGEC possesses relative lower T_g value, indicating the stronger intermolecular hydrogen bonding in PVC/PEHGEC than that of PVC/P*n*BGEC binary blends. Further increasing PEHGEC composition at 20 wt%, the single T_g value exhibited at 47 °C,

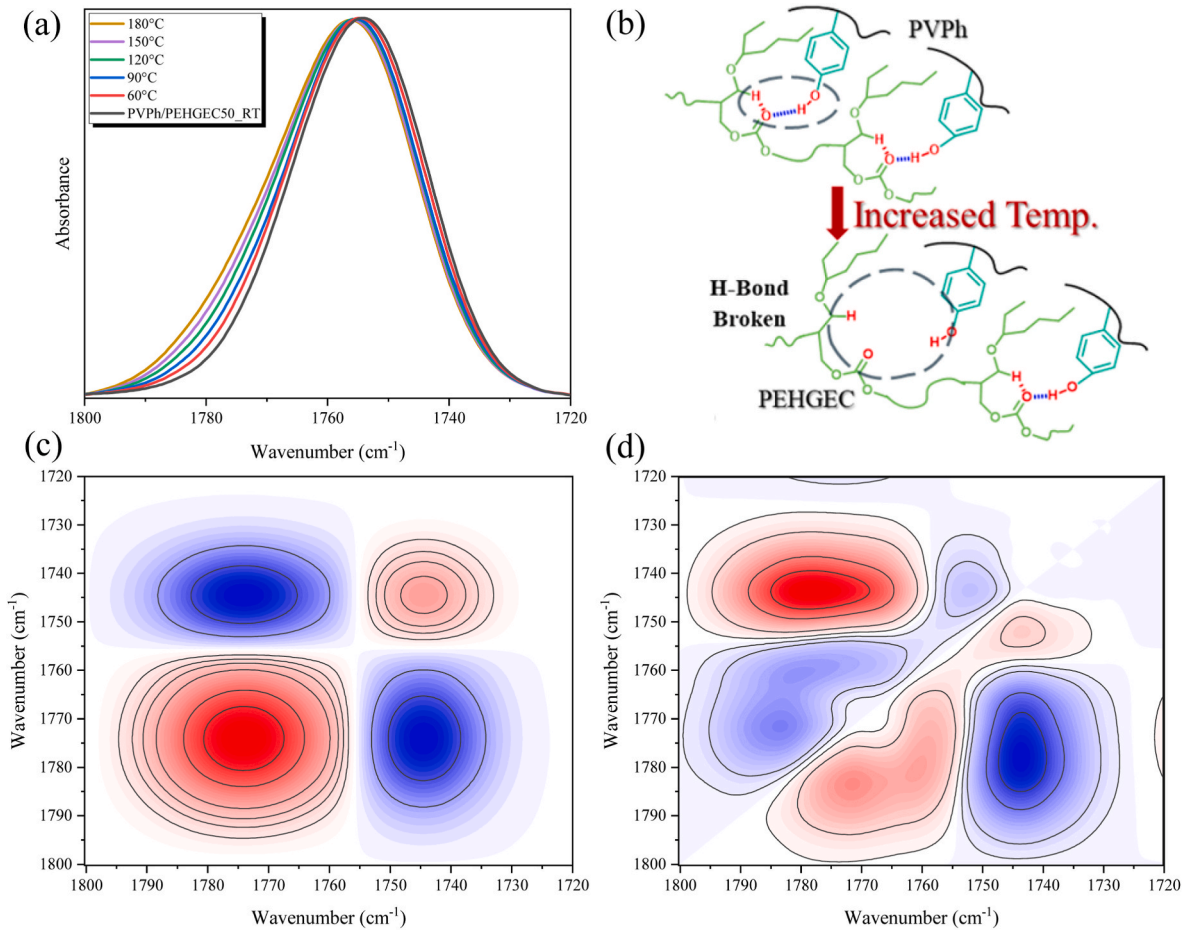

Fig. 10. (a) FTIR spectra of PVPh/PEHGEC = 50/50 blend recorded at various temperatures, (b) the possible interaction in PVPh/PEHGEC blends, (c) 2D FTIR synchronous and (d) asynchronous correlation maps.

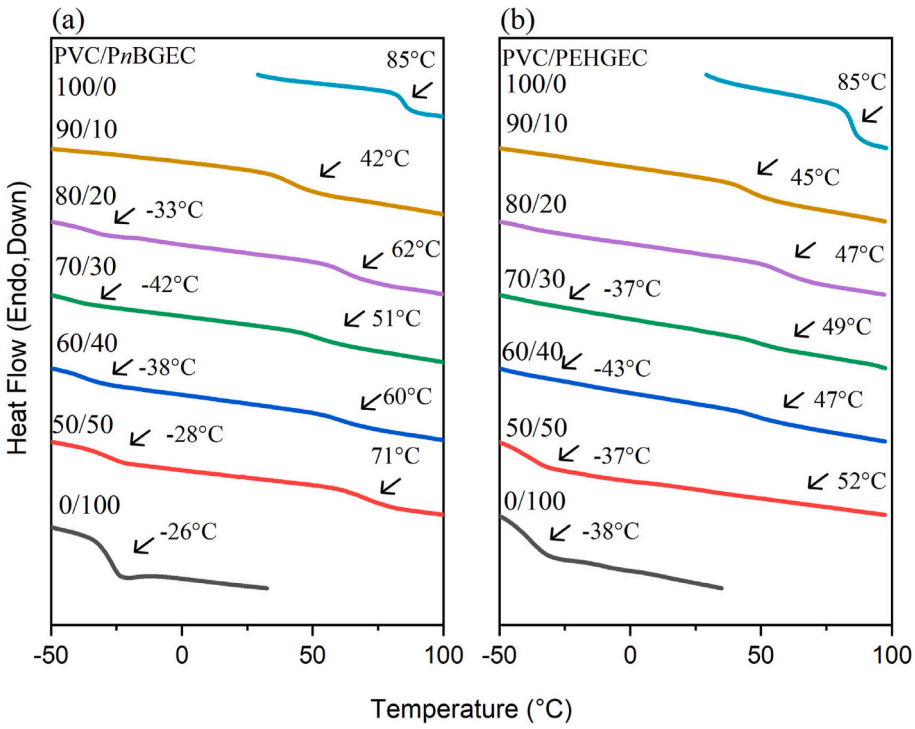

Fig. 11. DSC thermal analyses of (a) PVC/P*n*BGEC and (b) PVC/PEHGEC binary blends.

which is close to the value predicted by the Fox equation (51 °C), also indicating the miscible behavior. Further increasing PEHGEC compositions from 30 wt% to 50 wt%, although the second T_g behavior was not observed, the T_g value did not shift a lot, indicating that partial miscibility may occur at these blend compositions. Overall, the strength of intermolecular hydrogen bonding in PVC/PEHGEC binary blends is weaker than that of PVPh/PEHGEC binary blends, as also expected. Fig. S23 displays their corresponding FTIR spectra recorded at room temperature for PVC/P*n*BGEC and PVC/PEHGEC binary blends. Similarly, the C=O units from P*n*BGEC and PEHGEC segments in both binary blends also exhibit the peak shift, and the FWHM was changed after blending with PVC. We also expected that the intermolecular hydrogen bonding strength or FWHM should be smaller than that of the PVPh blending system. To further enhance the miscibility of PVC binary blends with CO_2-based alternating copolymer, the polyester segments should be incorporated into the CO_2-based alternating copolymer from anhydride monomer. For example, we observed that incorporating phthalic anhydride (PA) or 1,2-cyclohexanedicarboxylic anhydride (CHA) into PCHC to produce PCHC-PA or PCHC-CHA copolymers enhanced miscibility with PVPh, as the OH–ester interactions form stronger intermolecular hydrogen bonds than the OH-carbonate interactions [28]. As a result, Meng et al. proposed that poly (carbonate-ester) formed from PO and PA monomers with CO_2 could exhibit complete miscibility with PVC, as determined by dynamic mechanical analysis (DMA) [29]. Overall, this study provides the general principle to improve the miscibility behavior of CO_2-based copolymers through structural design by considering the intermolecular hydrogen bonding strength, free volume effect, and conformation entropy effect with weaker polar polymers such as PVC or strong self-association hydrogen bonding polymers such as PVPh.

4. Conclusions

We have successfully synthesized a series of CO_2-based alternating copolymers, including PPC, P*n*BGEC, PtBGEC, and PEHGEC, using a salen Co-Cl catalyst. The length of the side chains had a significant impact on the properties of the copolymers, and the T_g values of these copolymers were influenced by the side chain length, with longer side chains leading to lower T_g values because of a larger free volume effect. Through 1D- and 2D-FTIR spectroscopy, we observed the influence of side chains on the intramolecular hydrogen bonding interactions. Longer side chains weakened the intramolecular hydrogen bonding, as indicated by shifts in the C=O stretching bands and changes in the FWHM of these bands. This reduction in hydrogen bonding correlated with the decrease in T_g values. The binary polymer blends of PVPh with these CO_2-based copolymers indicate that the miscibility of the blends was found to be intensely dependent on the type and length of the side chains in the copolymers. The PVPh/PEHGEC blend exhibited the best miscibility, as indicated by a single T_g and the formation of stronger intermolecular hydrogen bonding interactions. In contrast, PVPh/PtBGEC and PVPh/PnBGEC blends were partially miscible or immiscible due to weaker intermolecular hydrogen bonding interactions. These results suggest that the presence of longer side chains in the copolymer chains influences the miscibility of the blends, likely due to changes in the intermolecular interactions and free volume effects. Furthermore, the study demonstrated that the strength of intermolecular hydrogen bonding in PVC-based binary blends (PVC/P*n*BGEC and PVC/PEHGEC) was weaker compared to PVPh-based blends, with the PVC/PEHGEC blend exhibiting a more favorable miscibility due to stronger hydrogen bonding interactions. These findings underline the importance of side chain length, hydrogen bonding, and free volume effects in controlling the miscibility behavior of polymer blends. In conclusion, this study provides valuable insights into the synthesis and design of CO_2-based copolymers and their blending behavior with other polymers, such as PVPh and PVC. The results highlight the crucial role of structural design in achieving improved miscibility and thermal properties in polymer blend systems. Further work is needed to explore incorporating other functional groups, such as ester groups, to enhance further the miscibility and performance of CO_2-based copolymers in diverse applications.

CRediT authorship contribution statement

Min-Jhen Yu: Writing – original draft, Investigation, Formal analysis, Data curation. **Yen-Ling Kuan:** Writing – original draft,

Methodology, Investigation, Conceptualization. **Wei-Ting Du:** Methodology, Investigation, Conceptualization. **Shiao-Wei Kuo:** Writing – review & editing, Writing – original draft, Supervision, Formal analysis, Conceptualization.

Declaration of competing interest

The authors declare that they have no known competing financial interests or personal relationships that could have appeared to influence the work reported in this paper.

Acknowledgments

This study was supported financially by the National Science and Technology Council, Taiwan, under contracts NSTC 113-2218-E-110-004 and 114-2223-E-110-001.

Appendix A. Supplementary data

Supplementary data to this article can be found online at https://doi.org/10.1016/j.polymer.2025.129550.

Data availability

Data will be made available on request.

References

[1] M. Echeverri, E.M. Maya, D.M. Munoz, Formation of bio-based cyclic carbonates from CO_2 and renewable feedstocks via porous poly(azomethine) -based heterogeneous catalysts approach, J. CO_2 Util. 90 (2024) 102977, https://doi.org/10.1016/j.jcou.2024.102977.

[2] J.G. Rosenboom, R. Langer, G. Traverso, Bioplastics for a circular economy, Nat. Rev. Mater. 7 (2022) 117–137, https://doi.org/10.1038/s41578-021-00407-8.

[3] K. Babaremu, O. Oladijo, E. Akinlabi, Biopolymers: a suitable REPLACEMENT for plastics in product packaging, Adv. Ind. Eng. Polym. Res. 6 (2023) 333–340, https://doi.org/10.1016/j.aiepr.2023.01.001.

[4] B. Song, A. Qin, B.Z. Tang, Syntheses, properties, and applications of CO_2-based functional polymers, Cell Rep. Phys. Sci. 3 (2022) 100719, https://doi.org/10.1016/j.xcrp.2021.100719.

[5] G.W. Yang, Y.Y. Zhang, R. Xie, G.P. Wu, Scalable bifunctional organoboron catalysts for copolymerization of CO_2 and epoxides with unprecedented efficiency, J. Am. Chem. Soc. 142 (2020) 12245–12255, https://doi.org/10.1021/jacs.0c03651.

[6] S. Sarkar, S.S. Roy, S. Krishnaswamy, D. Chakraborty, Phenoxy-imine supported hexacoordinate tetravalent titanium compounds: synthesis, characterization and catalytic applications for ROP and ROCOP reactions, Eur. Polym. J. 216 (2024) 113281, https://doi.org/10.1016/j.eurpolymj.2024.113281.

[7] W.T. Du, S.Y. Chen, S.W. Kuo, Mesoporous phenolic/carbon materials templated by CO_2-based PEO-*b*-PCHC diblock copolymers through mediated competitive intermolecular hydrogen bonding interactions for CO_2 capture, J. CO_2 Util. 80 (2024) 102702, https://doi.org/10.1016/j.jcou.2024.102702.

[8] Z. Huang, Y. Wang, N. Zhang, L. Zhang, D.J. Darensbourg, One-pot synthesis of ion-containing CO_2-based polycarbonates using protic ionic liquids as chain transfer agents, Macromolecules 51 (2018) 9122–9130, https://doi.org/10.1021/acs.macromol.8b01834.

[9] J. Marbach, B. Nörnberg, A.F. Rahlf, G.A. Luinstra, Zinc glutarate-mediated copolymerization of CO_2 and PO–parameter studies using design of experiments, Catal. Sci. Technol. 7 (2017) 2897–2905, https://doi.org/10.1039/C7CY00383H.

[10] S. Klaus, M.W. Lehenmeier, E. Herdtweck, P. Deglmann, A.K. Ott, B. Rieger, Mechanistic insights into heterogeneous zinc dicarboxylates and theoretical considerations for CO_2–epoxide copolymerization, J. Am. Chem. Soc. 133 (2011) 13151–13161, https://doi.org/10.1021/ja204481w.

[11] Q. Meng, R. Cheng, J. Li, T. Wang, B. Liu, Copolymerization of CO_2 and propylene oxide using ZnGA/DMC composite catalyst for high molecular weight poly (propylene carbonate), J. CO_2 Util. 16 (2016) 86–96, https://doi.org/10.1016/j.jcou.2016.06.011.

[12] J.Y. Jeon, S.C. Eo, J.K. Varghese, B.Y. Lee, Copolymerization and terpolymerization of carbon dioxide/propylene oxide/phthalic anhydride using a (salen) Co(III) complex tethering four quaternary ammonium salts, Beilstein J. Org. Chem. 10 (2014) 1787–1795, https://doi.org/10.3762/bjoc.10.187.

[13] Y. Qin, X. Sheng, S. Liu, G. Ren, X. Wang, F. Wang, Recent advances in carbon dioxide based copolymers, J. CO2 Util. 11 (2015) 3–9, https://doi.org/10.1016/j.jcou.2014.10.003.

[14] C. Chen, Y. Gnanou, X. Feng, Ultra-productive Upcycling CO_2 into polycarbonate polyols via borinane-based Bifunctional Organocatalysts, Macromolecules 56 (2023) 892–898, https://doi.org/10.1021/acs.macromol.2c02243.

[15] J. Zhang, L. Wang, S. Liu, X. Kang, Z. Li, A Lewis pair as organocatalyst for one-pot synthesis of block copolymers from a mixture of epoxide, anhydride, and CO_2, Macromolecules 54 (2021) 763–772, https://doi.org/10.1021/acs.macromol.0c02647.

[16] Z.Q. Qin, C.M. Thomas, S. Lee, G.W. Coates, Cobalt-based complexes for the copolymerization of propylene oxide and CO_2: active and selective catalysts for polycarbonate synthesis, Angew. Chem., Int. Ed. 42 (2003) 5484–5487, https://doi.org/10.1002/anie.200352605.

[17] K. Nakano, T. Kamada, K. Nozaki, Selective formation of polycarbonate over cyclic carbonate: copolymerization of epoxides with carbon dioxide catalyzed by a cobalt (III) complex with a piperidinium end-capping arm, Angew. Chem., Int. Ed. 45 (2006) 7274–7277, https://doi.org/10.1002/anie.200603132.

[18] S. Cui, J. Borgemenke, Z. Liu, Y. Li, Recent advances of "soft" bio-polycarbonate plastics from carbon dioxide and renewable bio-feedstocks via straightforward and innovative routes, J. CO_2 Util. 34 (2019) 40–52, https://doi.org/10.1016/j.jcou.2019.05.027.

[19] Y.L. Kuan, W.T. Du, S.W. Kuo, Effect of polyhedral oligomeric silsesquioxane (POSS) nanoparticle on the miscibility and hydrogen bonding behavior of CO_2 based poly (cyclohexene carbonate) copolymers, J. Taiwan Inst. Chem. Eng. 153 (2023) 105214, https://doi.org/10.1016/j.jtice.2023.105214.

[20] Y. Li, H. Shimizu, Compatibilization by homopolymer: significant improvements in the modulus and tensile strength of PPC/PMMA blends by the addition of a small amount of PVAc, ACS Appl. Mater. Interfaces 1 (2009) 1650–1655, https://doi.org/10.1021/am900314k.

[21] K.W. Meereboer, A.K. Pal, M. Misra, A.K. Mohanty, Green composites from a bioplastic blend of Poly(3-hyroxybutyrate-co-3- hydroxyvalerate) and carbon dioxide-derived Poly(propylene carbonate) and filled with a corn ethanol-industry Co-product, ACS Omega 6 (2021) 20103–20111, https://doi.org/10.1021/acsomega.1c00763.

[22] S. Cui, L. Li, Q. Wang, Enhancing glass transition temperature and mechanical properties of poly (propylene carbonate) by intermacromolecular complexation with poly (vinyl alcohol), Compos. Sci. Technol. 127 (2016) 177–184, https://doi.org/10.1016/j.compscitech.2016.03.007.

[23] L. Song, Y. Li, X. Meng, T. Wang, Y. Shi, Y. Wang, S. Shi, L.Z. Liu, Crystallization, structure and significantly improved mechanical properties of PLA/PPC blends compatibilized with PLA-PPC copolymers produced by reactions initiated with TBT or TDI, Polymers 13 (2021) 3245, https://doi.org/10.3390/polym13193245.

[24] W. Li, J. Qin, S. Wang, D. Han, M. Xiao, Y. Meng, Macrodiols derived from CO2-based polycarbonate as an environmentally friendly and sustainable PVC plasticizer: effect of hydrogen-bond formation, ACS Sustain. Chem. Eng. 6 (2018) 8476–8484, https://doi.org/10.1021/acssuschemeng.8b00735.

[25] X. Dong, L. Liu, Y. Wang, T. Li, Z. Wu, H. Yuan, P. Ma, D. Shi, M. Chen, W. Dong, The compatibilization of poly (propylene carbonate)/poly (lactic acid) blends in presence of core-shell starch nanoparticles, Carbohydr. Polym. 254 (2021) 117321, https://doi.org/10.1016/j.carbpol.2020.117321.

[26] T. Yu, Y. Zhou, Y. Zhao, K.P. Liu, E.Q. Chen, D.J. Wang, F.S. Wang, Hydrogen-bonded thermostable liquid crystalline complex formed by biodegradable polymer and amphiphilic molecules, Macromolecules 41 (2008) 3175–3180, https://doi.org/10.1021/ma7020562.

[27] H. Zuo, J. Liu, D. Huang, Y. Bai, L. Cui, L. Pan, K. Zhang, H. Wang, Sustainable and high-performance ternary blends from polylactide, CO_2 -based polyester and microbial polyesters with different chemical structure, J. Polym. Sci. 59 (2021) 1578–1595, https://doi.org/10.1002/pol.20210175.

[28] Y.L. Kuan, C.W. Chu, W.T. Du, S.W. Kuo, Design chemical structures of CO_2-Derived poly (cyclohexene carbonate) copolymers to mediate Intra-/Intermolecular interactions with strong hydrogen-bonded donor homopolymer, Macromolecules 58 (2025) 1090–1102, https://doi.org/10.1021/acs.macromol.4c02295.

[29] S. Chen, T. Zhao, P. Li, S. Wang, D. Han, S. Huang, W. Liu, Z. Huang, M. Xiao, Y. Meng, Biodegradable PVC plasticizer derived from a new CO_2-based Poly (carbonate-ester) macrodiol: molecular design and plasticizing effect, J. CO_2 Util. 80 (2024) 102695, https://doi.org/10.1016/j.jcou.2024.102695.

[30] A.D. Godwin, Plasticizers, Appl. Polym. Sci.: 21st Century (2000) 157–175, https://doi.org/10.1016/B978-008043417-9/50011-8.

[31] C.A. May, Epoxy Resins Chemistry and Technology, Marcel Dekker, New York, 1988.

[32] D.W. Van Krevelen, Properties of Polymers, Elsevier, Amsterdam, 1990.

[33] C.T. Cohen, T. Chu, G.W. Coates, Cobalt catalysts for the alternating copolymerization of propylene oxide and carbon dioxide: combining high activity and selectivity, J. Am. Chem. Soc. 127 (2005) 10869–10878, https://doi.org/10.1021/ja051744l.

[34] L.P. Nielsen, C.P. Stevenson, D.G. Blackmond, E.N. Jacobsen, Mechanistic investigation leads to a synthetic improvement in the hydrolytic kinetic resolution of terminal epoxides, J. Am. Chem. Soc. 126 (2004) 1360–1362, https://doi.org/10.1021/ja038590z.

[35] Y. Wang, Y. Zhao, S. Zhu, X. Zhou, J. Xu, X. Xie, R. Poli, Switchable polymerization triggered by fast and quantitative insertion of carbon monoxide into cobalt–oxygen bonds, Angew. Chem. Int. Ed. 132 (2020) 6044–6050, https://doi.org/10.1002/ange.201914216.

[36] D.D. Ford, L.P. Nielsen, S.J. Zuend, C.B. Musgrave, E.N. Jacobsen, Mechanistic basis for high stereoselectivity and broad substrate scope in the (salen) Co (III)-catalyzed hydrolytic kinetic resolution, J. Am. Chem. Soc. 135 (2013) 15595–15608, https://doi.org/10.1021/ja408027p.

[37] W.T. Du, Y.L. Kuan, S.W. Kuo, Intra-and intermolecular hydrogen bonding in miscible blends of CO_2/epoxy cyclohexene copolymer with poly (vinyl phenol), Int. J. Mol. Sci. 23 (2022) 7018, https://doi.org/10.3390/ijms23137018.

[38] I. Noda, Two-dimensional infrared spectroscopy, J. Am. Chem. Soc. 111 (1989) 8116–8118, https://doi.org/10.1021/ja00203a008.
[39] S.W. Kuo, W.J. Huang, C.F. Huang, S.C. Chan, F.C. Chang, Miscibility, specific interactions, and spherulite growth rates of binary poly(acetoxystyrene)/poly (ethylene oxide) blends, Macromolecules 37 (2004) 4164–4173, https://doi.org/10.1021/ma035417e.
[40] S.C. Chen, S.W. Kuo, C.S. Liao, F.C. Chang, Syntheses, specific interactions, and pH-sensitive micellization behavior of poly[vinylphenol-*b*-2-(dimethylamino) ethyl methacrylate] diblock copolymers, Macromolecules 41 (2008) 8865–8876, https://doi.org/10.1021/ma801546z.
[41] S.W. Kuo, H.C. Lin, W.J. Huang, C.F. Huang, F.C. Chang, Hydrogen bonding interactions and miscibility between phenolic resin and octa (acetoxystyryl) polyhedral oligomeric silsesquioxane (AS-POSS) nanocomposites, J. Polym. Sci., Part B: Polym. Phys. 44 (2006) 673–686, https://doi.org/10.1002/polb.20731.
[42] T.G. Fox, P.J. Flory, Second-order transition temperatures and related properties of polystyrene. I. Influence of molecular weight, J. Appl. Phys. 21 (1950) 581–591, https://doi.org/10.1063/1.1699711.
[43] A.A. Lin, T.K. Kwei, A. Reiser, On the physical meaning of the Kwei equation for the glass transition temperature of polymer blends, Macromolecules 22 (1989) 4112–4119, https://doi.org/10.1021/ma00200a052.
[44] D.E. Bugay, Characterization of the solid-state: spectroscopic techniques, Adv. Drug Deliv. Rev. 48 (2001) 43–65, https://doi.org/10.1016/S0169-409X(01)00101-6.
[45] Y. Tkachenko, P. Niedzielski, FTIR as a method for qualitative assessment of solid samples in geochemical research: a review, Molecules 27 (2022) 8846, https://doi.org/10.3390/molecules27248846.
[46] S.W. Kuo, Hydrogen Bonding in Polymeric Materials, Wiley-VCH Verlag GmbH & Co.KGaA, Weinheim, 2018.
[47] S.W. Kuo, Hydrogen bond-mediated self-assembly and supramolecular structures of diblock copolymer mixtures, Polym. Int. 58 (2009) 455–464, https://doi.org/10.1002/pi.2513.
[48] W.C. Chen, S.W. Kuo, U.S. Jeng, F.C. Chang, Self-assembly through competitive interactions of miscible diblock copolymer/homopolymer blends: poly (vinylphenol-b-methyl methacrylate)/poly (vinylpyrrolidone) blend, Macromolecules 41 (2008) 1401–1410, https://doi.org/10.1021/ma7021925.
[49] J. Kratochvíl, A. Šturcová, A. Sikora, J. Dybal, Interactions in a blend of two polymers greatly differing in glass transition temperature, J. Polym. Sci., Part B: Polym. Phys. 49 (2011) 1031–1040, https://doi.org/10.1002/polb.22272.
[50] C.J. Serman, P.C. Painter, M.M. Coleman, Studies of the phase behaviour of poly (vinyl phenol)-poly (n-alkyl methacrylate) blends, Polymer 32 (1991) 1049–1058, https://doi.org/10.1016/0032-3861(91)90591-6.